

The Bacterial 4S Pathway – A Benign and Economic Alternative for Crude Oil Desulphurization

J. Sousa, P. Ferreira, R. P. P. Neves, M. J. Ramos, P.A. Fernandes*

LAQV@REQUIMTE, Departamento de Química e Bioquímica, Faculdade de Ciências,

Universidade do Porto, Rua do Campo Alegre s/n, 4169-007 Porto, Portugal

* e-mail: pafernan@fc.up.pt

Modelling of DszA

Homology modelling

The DszA complex formed with oxidized flavin mononucleotide (DszA:FMN) was modelled as a tetramer with SwissModel¹ using the BdsA:FMN complex (PDB code: 5XKD)² as a template. The sequences from DszA and BdsA were aligned with the BLAST algorithm,³ and their similarity was scored with BLOSUM62 substitution matrix.⁴ The final model showed a root-mean-square deviation (RMSD) of 0.144 Å over 11,248 atoms (0.127 Å over 4,969 backbone atoms), a Global Model Quality Estimation of 0.92 out of 1.00 and a QMEAN score close to 0.0 (calculated -0.62).

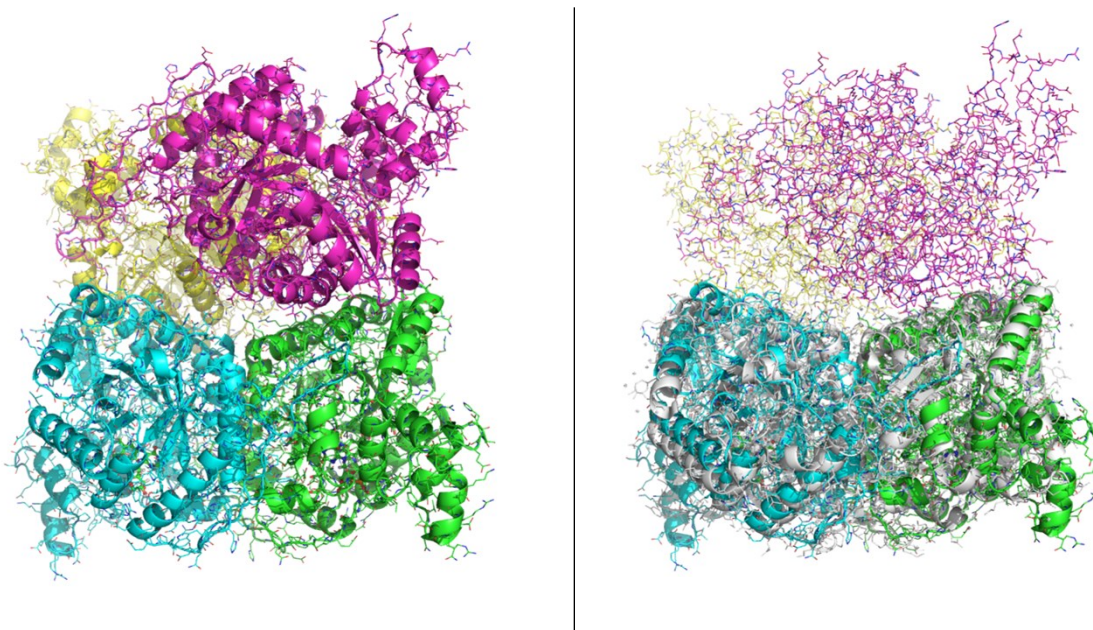


Figure S1. Left panel, DszA tetramer modelled from the BdsA tetramer (PDB ID: 5XKD). Right panel, superposition of the similar long-chain alkane monooxygenase (PDB ID: 3B9O, in white cartoon) with the modelled DszA tetramer.

From comparison with a similar long-chain alkane monooxygenase (PDB code: 3B9O, RMS of 1.694 Å over 4,865 atoms)⁵, the active form of DszA was assumed as a dimer.

Modelling of active DszA dimer in reactant and product state [DszA:C4A:FMN]

Each FMN in the dimer was modelled as C^{4a}-hydroperoxyflavin (C^{4a}OOH, chain A) and oxidized FMN (chain B). C^{4a}OOH and FMN were sculpted in PyMOL, with all heavy atoms with conserved hybridization kept restrained.

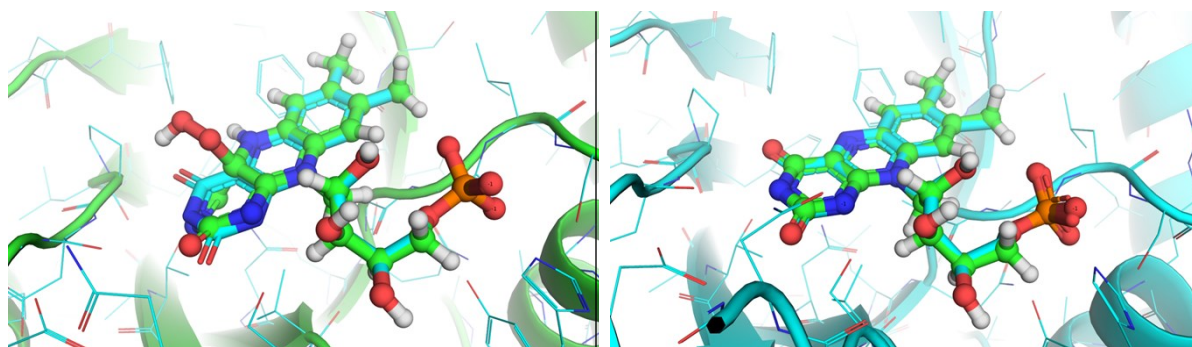


Figure S2. Left panel, C^{4a}OOH in ball-and-stick representation, modelled in chain A of DszA from X-ray coordinates of oxidized FMN (in cyan sticks). Right panel, oxidized FMN in ball-and-stick representation, modelled in chain B of DszA from X-ray coordinates of oxidized FMN (in cyan sticks).

The protonation states of the residues in the modelled dimer were assigned in their physiological state, following Propka3.1 predictions^{6, 7} and user structural inspection. In particular, for the assignment of the tautomer state for each His, user inspection was supported by predictions from the Gromacs pdb2gro module⁸⁻¹⁰ and the pdb2pqr server.^{11, 12}

Modelling the enzyme:substrate complexes [DszA:(C4A:DSN):(FMN:HBS)]

Since available X-ray structures of enzyme:FMN complexes are generally obtained with the oxidized FMN cofactor (which is a product of the reaction mechanism by DszA), both the substrate DBT-sulfone (DBTO₂) and the product 2-hydroxybiphenyl 2'-sulfinate (HBPS) were docked in each active site of the modelled dimer. The centre of the box was initially centred in the active site, as characterized for BdsA by Su and coworkers,² and then adjusted to include all sidechains of the residues in the active site and the C^{4a}OOH or FMN cofactor. Docking runs were performed with Autodock Vina 4.0 using the modelled DszA dimer in complex with C^{4a}OOH and FMN. 20 poses were generated using an exhaustiveness criteria of 20 and scoring energy within 4 kcal/mol.

From docking of DSN in chain A, poses no. 5, 6 and 15 were selected as these showed the lowest distance between the distal oxygen of C^{4a}OOH and one of the possible electrophilic carbons of DBTO₂, while also displaying different relative orientations to N⁵ of C^{4a}OOH and the catalytic His20 and His316.

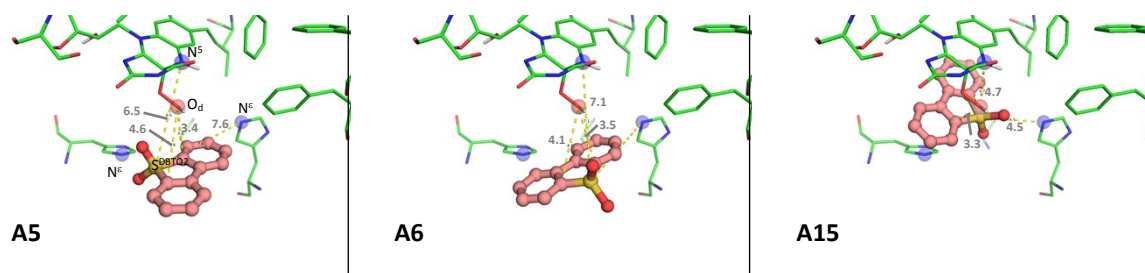


Figure S3. From left to right, depiction of docking poses 5, 6 and 15 for DBTO₂ (in pink ball-and-sticks), highlighting distances (in Å) that were particularly looked at to select docking poses, alongside the energy scoring criteria.

From docking of HBPS in chain B, pose no. 1, 3 and 16 were selected as representative of different orientations for HBPS. We particularly took into consideration the poses with different rotamers for the C-C axis of HBPS, and disregarded poses where differences were mostly translational.

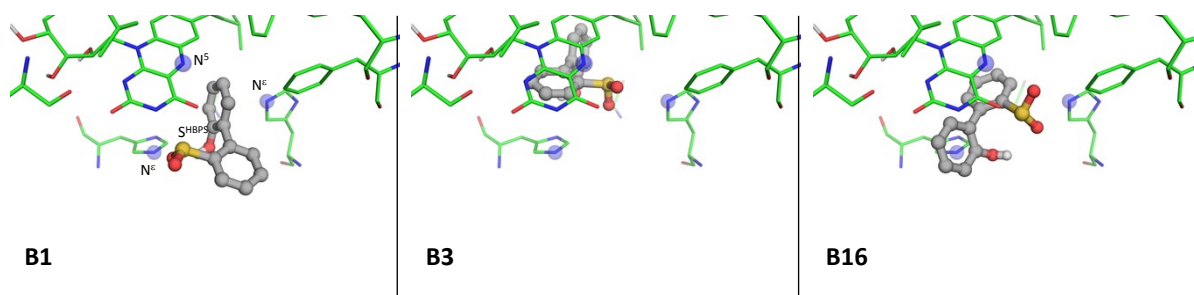


Figure S4. From left to right, depiction of docking poses 1, 3 and 16 for HBPS (in pink ball-and-sticks), highlighting in transparency spheres atoms that were particularly looked at to evaluate docking poses, alongside the energy scoring criteria.

Three out of nine DszA:(C^{4a}OOH: DBTO₂):(FMN:HBPS) models were initially generated: A5-B1, A6-B3 and A15-B16 (e.g. A5-B1 corresponds to chain A of the dimer holding pose 5 of DBTO₂ and chain B of the dimer holding pose 1 of HBPS). The models were solvated in a rectangular TIP3P¹³ water box with faces at least 12 Å from the DszA:(C^{4a}OOH: DBTO₂):(FMN:HBPS) complex. A total of 47 sodium counterions were then added to result in a unit cell with zero charge. The final system comprised 88 222 atoms.

Molecular dynamics simulations of enzyme:substrate complexes [DszA:(C4A:DSN):(FMN:HBS)]

Upon sequential energy minimization of modelled hydrogens, residue sidechains/ modelled substrates and the whole unit cell, a 50 ps annealing from 0–300 K and a 50 ps simulation in the canonical ensemble (*NVT*) were carried out with 2 kcal/(mol.Å²) harmonic restraints in backbone heavy atoms and a 1 fs timestep. Solvent density equilibration was carried out for 5 ns in the isothermal-isobaric ensemble (at 1 bar and 300 K), with a 2 fs timestep (using the LINCS algorithm^{14, 15} to constrain H-bonded atoms), the Berendsen modified thermostat and barostat.¹⁶ Finally, a total 55 ns simulation was run in the isothermal-isobaric ensemble (at 1 bar and 300 K), with a 2 fs timestep (using the LINCS algorithm to constrain H-bonded atoms), the modified Berendsen thermostat and the Parrinello-Rahman barostat.^{17, 18} A cut-off radius of 9 Å was used for particle-particle electrostatic and Lennard-Jones interactions. Beyond that radius, electrostatic interactions were treated with particle-mesh Ewald summations¹⁹ and Lennard-Jones interactions were truncated. All simulations were run with Gromacs 2018.3⁹.

References

1. T. Schwede, J. Kopp, N. Guex and M. C. Peitsch, *Nucleic Acids Res*, 2003, **31**, 3381-3385.
2. T. T. Su, J. Su, S. H. Liu, C. G. Zhang, J. He, Y. Huang, S. J. Xu and L. C. Gu, *Front Microbiol*, 2018, **9**.
3. C. Camacho, G. Coulouris, V. Avagyan, N. Ma, J. Papadopoulos, K. Bealer and T. L. Madden, *BMC Bioinformatics*, 2009, **10**.
4. S. Henikoff and J. G. Henikoff, *Proc Natl Acad Sci USA*, 1992, **89**, 10915-10919.
5. L. Li, X. Liu, W. Yang, F. Xu, W. Wang, L. Feng, M. Bartlam, M. Wang and Z. Rao, *J Mol Biol*, 2008, **376**, 453-465.
6. C. R. Sondergaard, M. H. M. Olsson, M. Rostkowski and J. H. Jensen, *J Chem Theor Comp*, 2011, **7**, 2284-2295.
7. M. H. M. Olsson, C. R. Sondergaard, M. Rostkowski and J. H. Jensen, *J Chem Theor Comp*, 2011, **7**, 525-537.
8. D. Van der Spoel, E. Lindahl, B. Hess, G. Groenhof, A. E. Mark and H. J. C. Berendsen, *J Comput Chem*, 2005, **26**, 1701-1718.
9. M. J. Abraham, T. Murtola, R. Schulz, S. Páll, J. C. Smith, B. Hess and E. Lindahl, *SoftwareX*, 2015, **1-2**, 19-25.
10. S. Páll, M. J. Abraham, C. Kutzner, B. Hess and E. Lindahl, Cham, 2015.
11. T. J. Dolinsky, P. Czodrowski, H. Li, J. E. Nielsen, J. H. Jensen, G. Klebe and N. A. Baker, *Nucleic Acids Res*, 2007, **35**, W522-W525.
12. T. J. Dolinsky, J. E. Nielsen, J. A. McCammon and N. A. Baker, *Nucleic Acids Res*, 2004, **32**, W665-W667.
13. W. L. Jorgensen, J. Chandrasekhar, J. D. Madura, R. W. Impey and M. L. Klein, *J Chem Phys*, 1983, **79**, 926-935.
14. B. Hess, *J Chem Theor Comp*, 2008, **4**, 116-122.
15. B. Hess, H. Bekker, H. J. C. Berendsen and J. G. E. M. Fraaije, *J Comput Chem*, 1997, **18**, 1463-1472.
16. H. J. C. Berendsen, J. P. M. Postma, W. F. Vangunsteren, A. Dinola and J. R. Haak, *J Chem Phys*, 1984, **81**, 3684-3690.
17. M. Parrinello and A. Rahman, *J Appl Phys*, 1981, **52**, 7182-7190.
18. S. Nose and M. L. Klein, *Mol Phys*, 1983, **50**, 1055-1076.
19. P. P. Ewald, *Ann Phys-Berlin*, 1921, **64**, 253-287.